On the Development of a Simple and Robust Active Control System for Boring Bar Vibration in Industry

Henrik Åkesson, Tatiana Smirnova, Ingvar Claesson and Lars Håkansson[†]

Department of Signal Processing, Blekinge University of Technology, 372 25 Ronneby, Sweden

Vibration in internal turning is a problem in the manufacturing industry. A digital adaptive controller for the active control of boring bar vibration may not be a sufficient solution to the problem. The inherent delay in a digital adaptive controller delays control authority and may result in tool failure when the load applied by the workpiece on the tool changes abruptly, e.g. in the engagement phase of the cutting edge. A robust analog controller, based on a lead-lag compensator, with simple adjustable gain and phase, suitable for the industry application, has been developed. Also, the basic principle of an active boring bar with embedded actuator is addressed. The performance and robustness of the developed controller has been investigated and compared with an adaptive digital controller based on the feedback filtered-x algorithm. In addition, this paper takes into account those variations in boring bar dynamics which are likely to occur in industry; for example, when the boring bars is clamped in a lathe. Both the analog and the digital controller manage to reduce the boring bar vibration level by up to approximately 50 dB.

[†] Member of the International Institute of Acoustics and Vibration (IIAV)

1. INTRODUCTION

Degrading vibrations in metal cutting e.g. turning, milling, boring and grinding are a common problem in the manufacturing industry. In particular, vibration in internal turning operations is a pronounced problem. To obtain the required tolerances of the workpiece shape, and adequate tool-life, the influence of vibration in the process of machining a workpiece must be kept to a minimum. This requires that extra care be taken in production planning and preparation. Vibration problems in internal turning have a considerable influence on important factors such as productivity, production costs, working environment, etc. In internal turning the dimensions of the workpiece hole will generally determine the length and limit the diameter or cross-sectional size of the boring bar. As a result, boring bars are frequently long and slender − long-overhang cantilever tooling- and thus sensitive to excitation forces introduced by the material deformation process in the turning operation.[1-3] The vibrations of a boring bar are often directly related to its low-order bending modes.[4-6]

The vibration problems in internal turning can be addressed using both passive and active methods.[1,2,7] Common methods used to increase dynamic stiffness of cantilever tooling involve making them (in high Young's modulus) nonductile materials, such as sintered tungsten carbide and machineable sintered tungsten, and/or utilising passive Tuned Vibration Absorbers (TVA).[1,2,8] These passive methods are known to enhance the dynamic stiffness and stability (chatter-resistance) of long cutting tools and thus, enable the allowable overhang to be increased.[1,2,8] The passive methods offer solutions with a fix enhancement of the dynamic stiffness frequently tuned for a narrow frequency range comprising a certain bending mode frequency that in some cases may be manually adjusted.[1,2,8] On the other hand, the active control of tool vibration enables a flexible solution that selectively increases the dynamic stiffness at the actual frequency of the dominating bending modes until the level of the chatter component in the feedback signal is negligible.[2,7,9] An active control approach was reported by Tewani et al.[10,11] concerning active dynamic absorbers in boring bars controlled by a digital state feedback controller. It was claimed to provide a substantial improvement in the stability of the cutting process. Browning et al.[12] reported an active clamp for boring bars controlled by a feedback version of the filtered-x LMS algorithm. They assert that the method enables to extend the operable length of boring bars. Claesson and Håkansson[9] controlled tool vibration by using the feedback filtered-x LMS algorithm to control tool shank vibration in the cutting speed direction without applying the traditional regenerative chatter theory.

Two important constraints concerning the active control of tool vibration involve the difficult environment in a lathe and industry demands. It is necessary to protect the actuator and sensors from the metal chips and cutting fluid. Also, the active control system should be applicable to a general lathe. Pettersson et al.[13] reported an adaptive active feedback control system based on a tool holder shank with embedded actuators and vibration sensors. This control strategy was later applied to boring bars by Pettersson et al.[6] Åkesson et al.[14] reported successful application of active adaptive control of boring bar vibration in industry using an active boring bar with embedded actuators and vibration sensors.

During the process of machining a workpiece in a lathe, the boundary conditions applied by the workpiece on the cutting tool may exhibit large and abrupt variation, particularly in the engagement phase between the cutting tool and workpiece. These abrupt changes of load applied by the workpiece on the tool may result in tool failure. However when utilising

active adaptive digital control of tool vibration, the problem of tool failure in the engagement phase may remain. For instance, the time required for the adaptive tuning of the controller, the inherent delay in, controller processing time, A/D and D/A-conversion processes, and analog anti-aliasing and reconstruction filtering might impede an active adaptive digital control system to produce control authority sufficiently fast to avoid tool failure. To provide means to address the issue of delay in control authority in the active control of boring bar vibration in industry an analog controller approach is suggested.

This article focuses on the development of a simple adjustable robust analog controller, based on digitally controlled analog design, that is suitable for the control of boring bar vibration in industry. Initially a digitally controlled analog manually adjustable lead compensator was developed. To provide more appropriate controller responses a manually adjustable bandpass lead-lag compensator was developed. Gain and phase of the controller response may, at a selectable frequency, be independently adjusted on the two developed controller prototypes. Also, the performance and robustness using the two analog controllers was evaluated and compared with a digital adaptive controller based on the feedback filtered-x LMS-algorithm[15,16] in the active control of boring bar vibration.

2. MATERIALS AND METHODS

2.1. Experimental Setup

Experiments concerning active control of tool vibration have been carried out in a Mazak SUPER QUICK TURN - 250M CNC turning centre. The CNC lathe, presented by the photo in Fig. 1, shows the room in the lathe in which the machining is carried out. In this photo (Fig. 1(b)), the turret configured with a boring bar clamped in a clamping house, and a workpiece clamped in the chuck are observable.

A coordinate system was defined: z was in the feed direction, y in the reversed cutting speed direction, and x in the cutting depth direction (see upper left corner of Fig. 1(b)).

Work material − cutting data − tool geometry. The cutting experiments used the work material chromium molybdenum nickel steel SS 2541-03 (AISI 3239). The material deformation process of this material during turning excites the boring bar with a narrow bandwidth and has a susceptibility to induce severe boring bar vibration levels,[4,5] resulting in poor surface finish, tool breakage, and severe acoustic noise levels. The workpiece used in the cutting experiments had a diameter of 225 mm and a length of 230 mm. To enable supervision of the metal-cutting process during continuous turning, the cutting operation was performed externally, see Fig. 1(b). An active boring bar was firmly clamped in a clamping house rigidly attached to the lathe turret. Only one side of the workpiece shaft's end was firmly clamped into the chuck of the lathe, see Fig. 1(b). As a cutting tool, a standard 55° diagonal insert with geometry DNMG 150608-SL and carbide grade TN7015 for medium roughing was used. The following cutting data was selected: Cutting speed $v = 60$ m/min, Depth of cut $a = 1.5$ mm, and Feed $s = 0.2$ mm/rev.

Measurement equipment and setup. A block diagram of the experimental setup for the active control of boring bar vibrations is presented in Fig. 2.
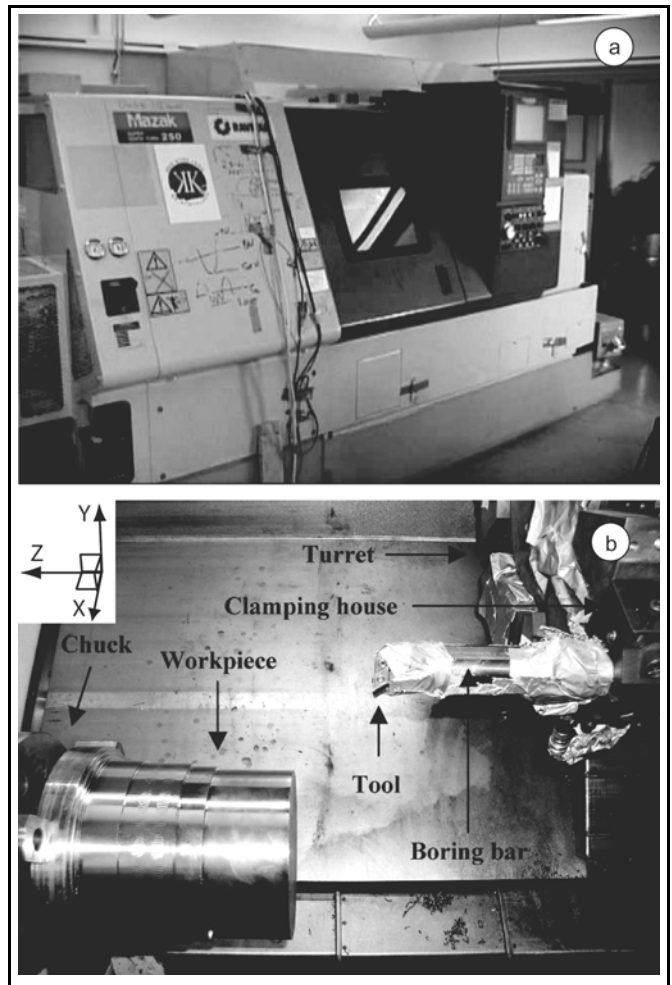

Figure 1. (a) Mazak SUPER QUICK TURN - 250M CNC lathe and (b) the room in the lathe where the machining is carried out.
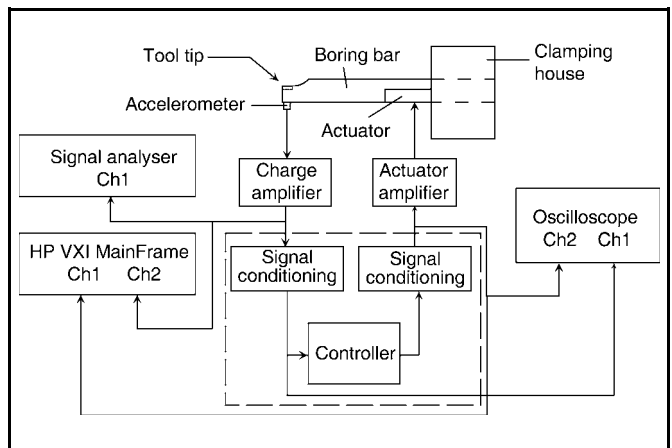

Figure 2. A block diagram describing the experimental setup for the active vibration control system.

The control experiments used an active boring bar equipped with an accelerometer and an embedded piezoceramic stack actuator. The actuator was powered with an actuator amplifier, custom designed for capacitive loads, and the accelerometer was connected to a charge amplifier. A floating point signal processor with Successive Approximation Register AD- and DA- converters were used. Two commercial signal conditioning filters were used in the control experiments. A VXI Mainframe E8408A with two 16-channel 51.2 kSa/s cards were used for data collection.
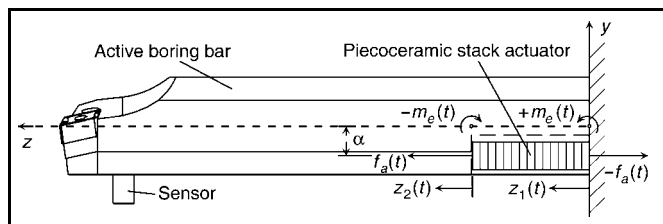
2.2. Active Boring Bar

The active boring bar used in this experiment is based on the standard WIDAX S40T PDUNR15 boring bar with an accelerometer and an embedded piezoceramic stack actuator. By embedding accelerometers and piezoceramic stack actuators in conventional boring bars, a solution for the introduction of control force to the boring bar with physical features and properties that fit the general lathe application may be obtained.

Active boring bar − simple model. A Euler-Bernoulli beam may be used as a simple model to illustrate the structural dynamic properties of a boring bar.[4,5] The Euler-Bernoulli differential equation describing the transversal motion in the y direction of the boring bar may be written as:[17-19]

$$\rho A(z)\frac{\partial^2 u(z,t)}{\partial t^2} + \frac{\partial^2}{\partial z^2}\left[EI(z)\frac{\partial^2 u(z,t)}{\partial z^2}\right] = \frac{\partial m_e(z,t)}{\partial z}, \quad (1)$$

where ρ is the density of the boring bar, $A(z)$ the cross-sectional area, $u(z,t)$ the deflection in y direction, E the Young's elastic modulus, $I(z)$ the cross-sectional area moment of inertia, and $m_e(z,t)$ the space- and time-dependent external moment load per unit length. The boundary conditions of the boring bar depend on the suspension of the boring bar ends, and a clamped-free model is suggested.[4,5,20] Figure 3 illustrates a boring bar with a piezoelectric stack actuator embedded in a milled space in the underside of the boring bar.

Figure 3. The configuration of the piezoceramic stack actuator in the active boring bar.

Assuming that the actuator operates well below its resonance frequency, thus neglecting inertial effects of the actuator. Then, in the frequency domain, the force the actuator exerts on the boring bar, $F_a(f)$ (the Fourier transform of $f_a(t)$ and f is frequency), may approximately be related to the constraint expansion or motion of the actuator, $Z(f) = Z_2(f) − Z_1(f)$, as $F_a(f) = K_a(\Delta L_a(f) − Z(f))$.[17] Where $Z_1(f)$ and $Z_2(f)$ are the Fourier transform of the displacements $z_1(t)$ and $z_2(t)$, $\Delta L_a(f)$ is the Fourier transform of the free expansion of an unloaded piezoelectric stack actuator[17] and K_a is the actuator equivalent spring constant. If the point receptance at the respective actuator end are summed to form the receptance $H_B(f) = Z_1(f)/F_a(f) + Z_2(f)/F_a(f)$, the relative displacement $Z(f)$ may be expressed $Z(f) = H_B(f)F_a(f)$. With the aid of Newton's second law, an expression for the actuator force applied on the boring bar as a function of the actuator voltage $V(f)$ may now be written as:[17]

$$F_a(f) = H_{fv}(f)V(f), \quad (2)$$

where $H_{fv}(f)$ is the electro-mechanic frequency function between input actuator voltage $V(f)$ and output actuator force $F_a(f)$. The distance between the actuator − boring bar inter-face centre and the natural surface of the active boring bar in the y-direction is α (see Fig. 3). Thus, the external moment per unit length applied on the boring bar by the actuator force $F_a(f)$ may be approximated as:

$$m_e(z,f) = \alpha F_a(f)(\delta(z − z_1) − \delta(z − z_2))), \quad (3)$$

where $\delta(z)$ is the Dirac delta function and z_1 respective z_2 are the z-coordinates for the actuator − boring bar interfaces. Based on the method of eigenfunction expansion,[21] if $z_1 = 0$ the generalised load of mode r is $F_{load,r}(f) = \alpha F_a(f)\psi'_r(z_2)$, ψ'_r is the derivative of the normal mode r. Expressing the generalised load with the aid of Eq. (2) and relying on the method of eigenfunction expansion,[21] the frequency-domain dynamic response of the boring bar in the y direction may be written as:

$$u(z,f) = \sum_{r=1}^{\infty} \psi_r(z)H_r(f)\alpha H_{fv}(f)V(f)\psi'_r(z_2), \quad (4)$$

where $H_r(f)$ is the frequency response function and ψ_r is the normal mode, for mode r.

2.3. System Identification

The design of feedback controllers usually rely on detailed knowledge of the dynamic properties of the system to be controlled, e.g. a dynamic model of the system to be controlled.[22,23] Non-parametric spectrum estimation may be utilised to produce non-parametric linear least-squares estimates of dynamic systems.[23,24] Welch spectrum estimator[25] was used and Table 1 column A gives the spectral density estimation parameters used in the production of plant frequency function estimates, with various clamping conditions for the boring bar. Also, the spectral density estimation parameters used in the production of plant frequency function estimates during continuous metal cutting can be found in Table 1 column B. In Table 1 column C, the spectral density estimation parameters used in the production of frequency function estimates for the controller responses are given, and in Table 1 column D, the spectrum estimation parameters used for the production of power spectral density estimates for boring bar vibration with and without active control are presented.

Table 1. Spectral density estimation parameters used for the production of boring bar vibration spectra, with and without active control.

Parameter	A	B	C	D
Excitation signal	Burst rand.	True rand.	True rand.	Cutting proc.
Sampling frequency f_s (Hz)	8192	10240	10240	10240
Block length N	16384	20480	20480	10240
Frequency resolution Δf (Hz)	0.5	0.5	0.5	1
Number of averages L	160	265-635	160	100
Burst length	90%	–	–	–
Frequency range of burst (Hz)	0-4000	–	–	–
Window $w(n)$	Rectangular	Hanning	Hanning	Hanning
Overlap	0%	50%	50%	50%

2.4. Controllers

The application of active control of boring bar vibration in industry requires reliable robust adaptive feedback control or manually tuned feedback control, which is simple to adjust at the shop floor by the lathe operator. A controller suitable for active control of boring bar vibrations might be implemented using different approaches. However, the abrupt changes that occur in the turning operations, i.e. in the engagement phase, suggest that an analog control approach might be suitable with respect to, for example, the controller delay and thus delay in control authority. Simple and effective compensators or controllers that may be implemented in the analog domain are the lag and lead compensators that approximate the PI controller and the PD controller, respectively. Moreover, the PID controller may be approximated in the analog domain by combining a lag compensator with a lead compensator.[26]

A block diagram of the active boring bar vibration feedback control system, a feedback control system for disturbance rejection, is presented in Fig. 4 where $-W$ is the controller, $y(t)$ is the controller output signal, C is the plant or control path, $y_c(t)$ is the plant output vibration (secondary vibration), $d(t)$ is the undesired tool vibration, and $e(t)$ is the error signal.
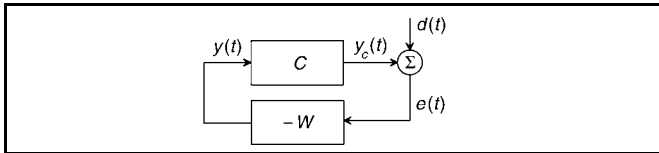
Figure 4. Block diagram of the active tool vibration control system.

If the plant and the controller are linear time invariant stable systems, their dynamic properties may be described by the frequency response functions $C(f)$ and $W(f)$, respectively. Then, the feedback control systems' open-loop frequency function can be written as $H_{ol}(f) = W(f)C(f)$ and the closed-loop frequency function for the active boring bar vibration feedback control system is given by $H_{cl}(f) = 1/(1 + W(f)C(f))$.

Controller performance and robustness. Principally, there are two important aspects of the behaviour of feedback controllers in active control systems, their performance and their robustness; that is, the ability of the controller to reject disturbance and to remain stable under varying conditions.[22] Basically, good performance in feedback control requires high loop gain; while on the other hand, robust stability usually implies a more retained loop gain. Usually, the discussion concerning the performance and robust stability of feedback controllers is based on the sensitivity function $S(f) = 1/(1 + W(f)C(f))$ and the complementary sensitivity function $T(f) = W(f)C(f)/(1 + W(f)C(f))$.[22,23] The sensitivity function $S(f)$ gives a measure on disturbance reduction of a feedback control system. In the determination of the stability properties of the system, the complementary sensitivity function $T(f)$ has a vital role. It also governs the performance of the control system regarding the reduction of noise from the sensor detecting the error $e(t)$. Generally, the design of controllers rely on a model of the system to be controlled or the so called plant. However, a model of a physical system is an approximation of the true dynamics of the system and it is therefore likely to affect the performance of the control

system.[22,23] To incorporate the plant uncertainty in the design procedure of a controller, a model of the plant uncertainty is usually included. A common way to model the plant uncertainty is with a multiplicative perturbation, yielding a frequency function model of the plant as:[22,23,27]

$$C_{actual}(f) = C_{nominal}(f)(1 + \Delta_C(f)), \quad (5)$$

where $\Delta_C(f)$ is an unstructured perturbation given by:

$$\Delta_C(f) = \frac{C_{actual}(f)}{C_{nominal}(f)} - 1, \quad (6)$$

and $C_{nominal}(f)$ is a nominal plant model of the plant. Thus, assuming that a control system design based on the nominal plant model results in a theoretically stable control system, then the denominator $1 + W(f)C_{nominal}(f)$ has no zeros in the right half complex plane. However, the actual control system's frequency response function will have the denominator $1 + W(f)C_{actual}(f)$. Thus, if $|1 + W(f)C_{nominal}(f)| > |W(f) \times C_{nominal}(f)\Delta_C(f)|, \forall f$ is fulfilled, the actual control system is stable.[22,28,29] Hence, for stable control the unstructured perturbation is upper limited as $|\Delta_C(f)| < 1/|T_{nominal}(f)|, \forall f$ where $T_{nominal}(f) = W(f)C_{nominal}(f)/(1 + W(f)C_{nominal}(f))$. If $\Delta_C(f)$ is bounded as $|\Delta_C(f)| \leq \beta(f), \forall f$. The condition for robust stability of a control system is given by:[28]

$$\beta(f) < \frac{1}{|T_{nominal}(f)|}, \forall f. \quad (7)$$

The performance and robustness of an active feedback control system may also be visualised by a polar plot of its open-loop frequency response function in a Nyquist diagram.[22,28,29] If the closed loop system is to be stable, the polar plot of the open loop frequency response for the feedback control system $W(f)C(f)$ must not enclose the polar coordinate $(-1, 0)$ in the Nyquist diagram. The larger the distance between the polar plot and the $(-1, 0)$ point, the more robust the feedback control system becomes, with respect to variation in plant response.

Compensators. A lead compensators purpose is to advance the phase of the open loop frequency response $W(f)C(f)$ for a feedback control system, usually by adding maximal positive phase shift in the frequency range where the loop gain equals 0 dB, i.e. at the crossover frequency.[26,29] This will increase the phase margin and generally increase the bandwidth of a feedback control system.[26,29] The characteristic equation or frequency function for a lead compensator may be written as:[30]

$$W_{Lead}(f) = K_{lead}\frac{1}{a_{lead}}\frac{j2\pi f + z_{lead}}{j2\pi f + p_{lead}} = K_{lead}\frac{\tau_{lead}j2\pi f + 1}{a_{lead}\tau_{lead}j2\pi f + 1}, \quad (8)$$

where $z_{lead} > 0$ and $z_{lead} \in \Re$ ($-z_{lead}$ is the compensator zero), $p_{lead} > 0$ and $p_{lead} \in \Re$ ($-p_{lead}$ is the compensator pole), $a_{lead} = z_{lead}/p_{lead} < 1$ is the inverse lead ratio for a lead compensator, K_{lead} is the compensator gain, and $\tau_{lead} = 1/z_{lead}$. By utilising a lag compensator, the low frequency loop gain of a feedback control system may be increased as the phase-lag filter attenuates the high frequency gain. In this way, the gain margin of the open loop frequency response for the feedback

control system can be improved, and the phase shift added by the compensation filter can be minimised.[26,28,29] The characteristic equation or frequency function for a lag compensator is fairly similar to the lead compensator characteristic equation and may be expressed as:[30]

$$W_{Lag}(f) = K_{lag} \frac{1}{a_{lag}} \frac{j2\pi f + z_{lag}}{j2\pi f + p_{lag}} = K_{lag} \frac{\tau_{lag} j2\pi f + 1}{a_{lag}\tau_{lag} j2\pi f + 1}, \quad (9)$$

where $z_{lag} > 0$ and $z_{lag} \in \Re$ ($-z_{lag}$ is the compensator zero), $p_{lag} > 0$ and $p_{lag} \in \Re$ ($-p_{lag}$ is the compensator pole), $a_{lag} = z_{lag}/p_{lag} > 1$ is the inverse lag ratio for a lag compensator, K_{lag} is the compensator gain, and $\tau_{lag} = 1/z_{lag}$.

A lead-lag compensator is obtained by connecting a lead compensator and a lag compensator in series, thus by combining Eqs. (8) and (9). The lag compensator may be adjusted to provide a suitable low frequency loop gain of the feedback control system. Subsequently, the lead compensator may be adjusted to provide an additional positive phase shift in the frequency range, where the loop gain equals 0 dB, i.e. at the crossover frequency.[26,29]

Digitally controlled analog controller. The intention is to develop an analog controller with response properties that can be easily adjusted manually, without necessitating the replacement of discrete components, i.e. resistors and capacitances. If a lead compensator is considered, its frequency response function is given by Eq. (8).[26,29] A lead compensator may be designed according to the circuit diagram shown in Fig. 5, where $R_{d,2}$ and $R_{d,f}$ are adjustable resistors, $R_{d,1}$ is a fixed resistor and C_d is a fixed capacitor. The parameters in Eq. (8) are related to the discrete components as $K_{lead} = R_{d,f}/(R_{d,2} + R_{d,1})$, $\tau_{lead} = C_d R_{d,2}$, and $a_{lead} = R_{d,1}/(R_{d,2} + R_{d,1})$.
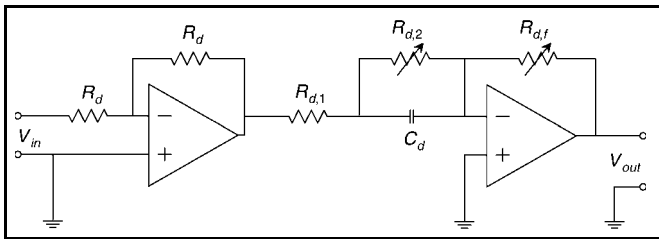

Figure 5. Circuit diagram of a lead compensator.

If $R_{d,2}$ and $R_{d,f}$ are implemented by digitally controlled potentiometers, the phase and gain of the compensator response may be adjusted independently at one selectable frequency, in discrete steps, to successively increase or decrease phase and gain respectively. For instance, by using two knobs for the compensator tuning (one for phase adjustment and one for gain adjustment) a function of the two knob angles may be produced according to:

$$[a, g] = AG_{lead}(gain\ knob\ angle,\ phase\ knob\ angle). \quad (10)$$

This function produces integers $a \in \{1, 2, ..., L_a\}$ and $g \in \{1, 2, ..., L_g\}$, selecting the appropriate analog compensator frequency response function in the set of $L_a \times L_g$ different analog compensator frequency response functions:

$$W_{lead;a,g}(f) = K_{a,g} \frac{\tau_{a,g} j2\pi f + 1}{a_{a,g}\tau_{a,g} j\omega + 1},$$

$$a \in \{1, 2, ..., L_a\} \text{ and } g \in \{1, 2, ..., L_g\}. \quad (11)$$

The micro-controller realised the *AG(gain knob angle, phase knob angle)* function, by controlling the adjustable resistors $R_{d,2}$ and $R_{d,f}$, (the so called digital potentiometers that have a digital control interface and an analog signal path). Such a micro-controller will allow the implementation of an analog lead-circuit which enabling orthogonal adjustment of the phase function and magnitude function at one selectable frequency of the compensator response. If the frequency for orthogonal adjustment of the phase function and magnitude function is set to 500 Hz, the magnitude and phase functions of the frequency response function realised by this circuit may be adjusted with the phase knob according to the 3-D plots in Fig. 6(a) and (b), respectively. Observe, the gain knob only adjusts the level of the magnitude function surface and has no influence on its shape or the shape of the phase function surface.
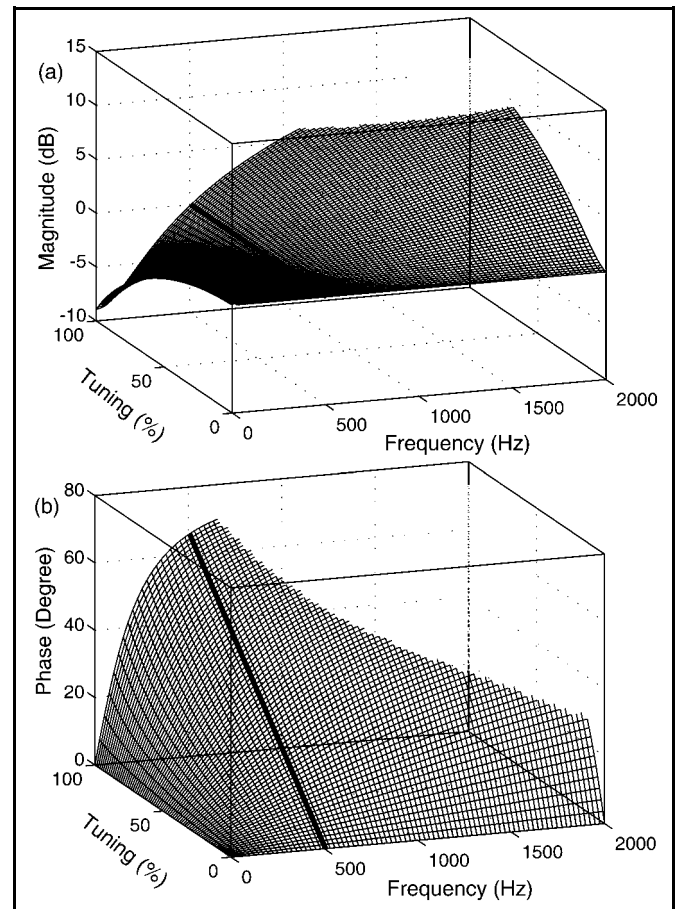

Figure 6. Magnitude function (a) and phase function (b) of lead compensator frequency response function as a function of phase knob adjustment range in % and frequency. The gain knob only adjusts the level of the magnitude function surface.

A lag compensator with orthogonal adjustment of the phase function and the magnitude function at one selectable frequency of the compensator response may be designed similar to the adjustable analog lead compensator. Thus, an adjustable lag compensator may be designed according to the circuit diagram shown in Fig. 7.

In Fig. 7, $R_{g,1}$ and $R_{g,f}$ are adjustable resistors and $R_{g,f}$ is a fixed resistor and C_g is a fixed capacitor. The frequency response function for the lag compensator is given by Eq. (9).[26,29] The parameters in the equation are related to the discrete components according to, $K_{lag} = \dfrac{R_{g,f}}{R_{g,1} + R_{g,3}}$,

$\tau_{lag} = C_g R_{g,2}$, and $\alpha_{lag} = \dfrac{R_{g,1} R_{g,2} + R_{g,1} R_{g,3} + R_{g,2} R_{g,3}}{R_{g,1} R_{g,2} + R_{g,2} R_{g,3}}$. In much the same way as the orthogonally adjustable lead compensator, a micro-controller realises an AG_{lag}(*gain knob angle, phase knob angle*) function suitable for steering the digital potentiometers implementing the adjustable resistors $R_{g,1}$ and $R_{g,f}$ for the lag compensator. If the frequency for orthogonal adjustment of the phase and magnitude functions is selected to 500 Hz, the magnitude and phase functions of the frequency response function realised by this circuit may be adjusted with the phase knob, according to the 3-D plots in Fig. 8(a) and (b), respectively.
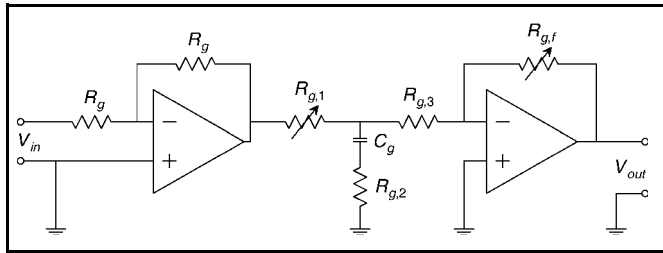

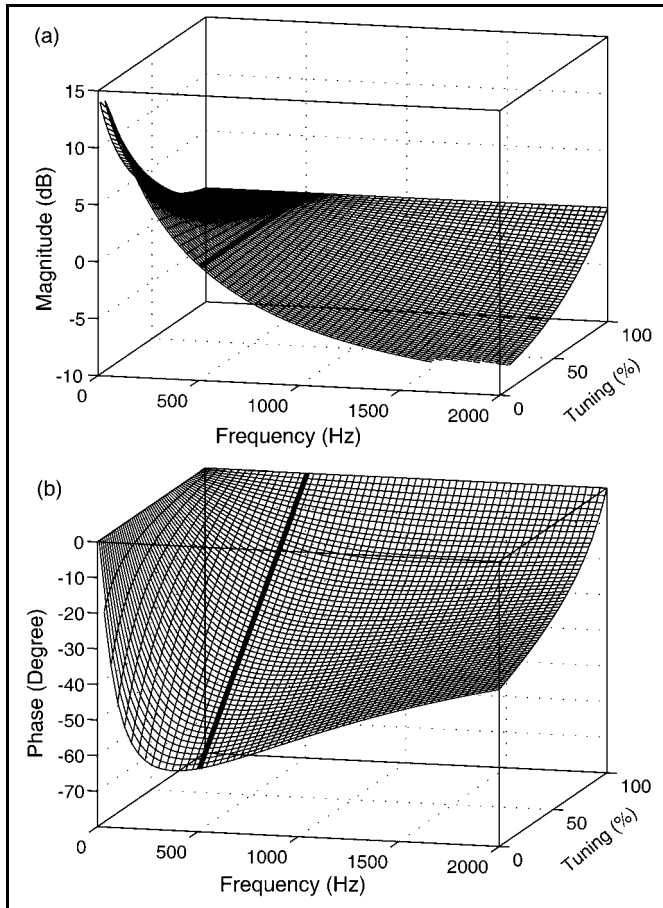**Figure 7.** Circuit diagram of a lag compensator.

Figure 8. Magnitude function (a) and phase function (b) of lag compensator frequency response function as a function of phase knob adjustment range in % and frequency. The gain knob only adjusts the level of the magnitude function surface.

By connecting the adjustable lead compensator in series with the adjustable lag compensator, a lead-lag compensator with orthogonal adjustment of the phase function and the magnitude function at one selectable frequency of the response may be realised. The magnitude and phase functions

of the lead-lag compensator may be adjusted with the phase knob e.g. according to the 3-D plots in Fig. 9(a) and (b) respectively.
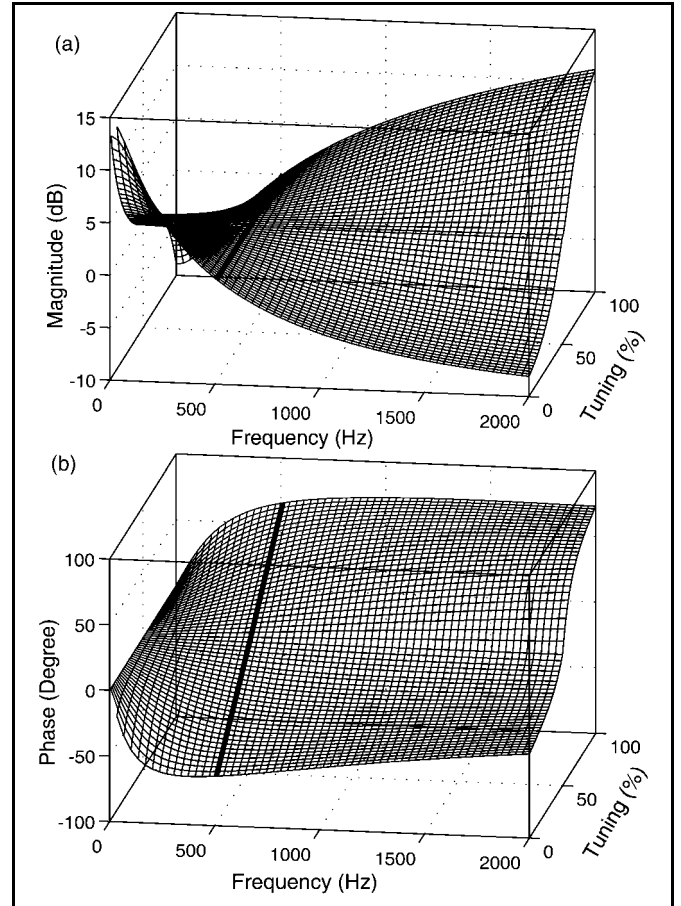

Figure 9. Magnitude function (a) and phase function (b) of lead-lag compensator frequency response function, as a function of phase knob adjustment range in % and frequency. The gain knob only adjusts the level of the magnitude function surface.
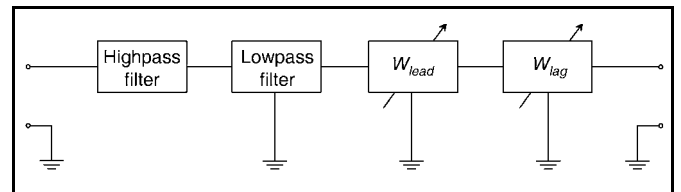

Figure 10. Block diagram of the implemented lead-lag circuit.

Also, to utilise the capacity of the actuator amplifier, to limit the active control frequency range, a suitable high-pass filter, followed by a suitable low-pass filter was connected in series with the lead-lag compensator. The block diagram of the obtained analog band-pass lead-lag controller is shown in Fig. 10.

Selecting the frequency for orthogonal adjustment of the phase and magnitude functions to 500 Hz, this controller's frequency response magnitude and phase functions are adjustable with the phase knob, according to the 3-D plots in Fig. 11(a) and (b), respectively.

The implemented analog lead-lag controller consists of several blocks: high-pass filter, low-pass filter, lead compensator and lag compensator. Each block can be used separately or arbitrary combinations of the blocks can be used to enable controller flexibility.
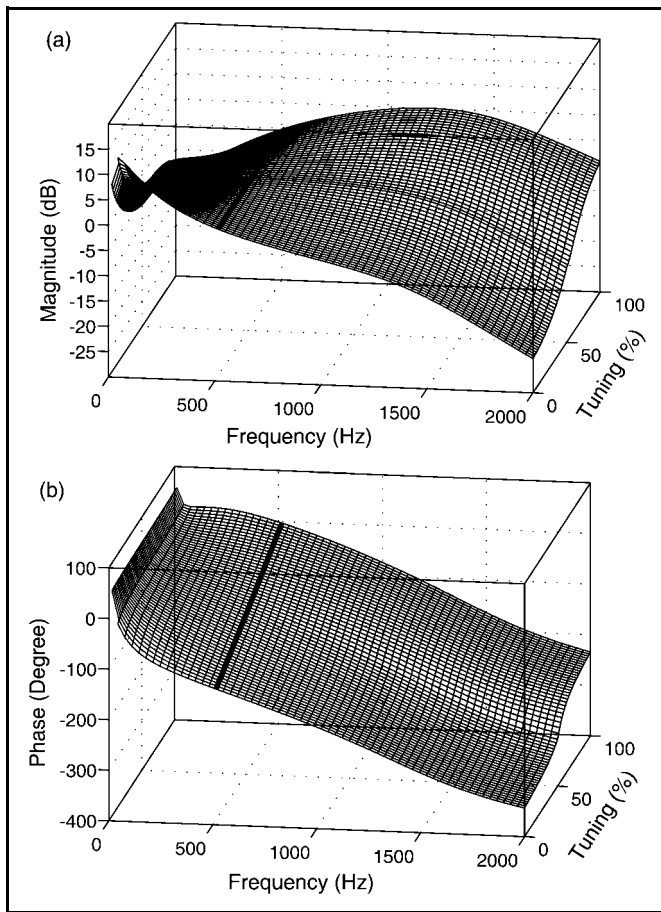
Figure 11. Magnitude function (a) and phase function (b) of band-pass lead-lag compensator frequency response function, as a function of phase knob adjustment range in % and frequency. The gain knob only adjusts the level of the magnitude function surface.

Feedback filtered-x LMS algorithm. The feedback filtered-x LMS algorithm is an adaptive digital feedback controller suitable for narrow-band applications.[15,16,31] This algorithm is based on the method of steepest descent and the objective of the control is to minimise the disturbance signal or desired signal in the mean square sense.[16,16,31] A block diagram of the feedback filtered-x LMS algorithm is shown in Fig. 12.
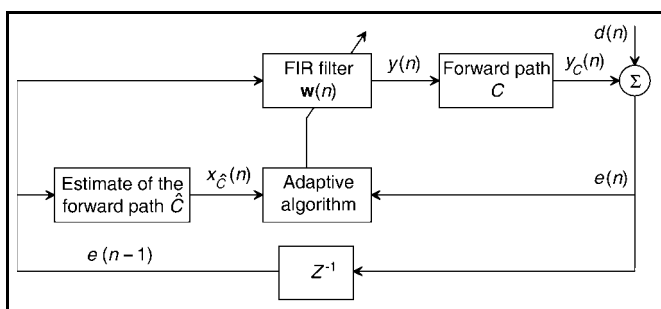
Figure 12. Block diagram of the feedback filtered-x LMS algorithm.

The feedback filtered-x LMS algorithm with leakage coefficient is defined by the following equations:

$$y(n) = \mathbf{w}^T(n)\mathbf{x}(n); \qquad (12)$$

$$e(n) = d(n) + y_C(n); \qquad (13)$$

$$\mathbf{w}(n+1) = \gamma \mathbf{w}(n) - \mu \mathbf{x}_{\hat{C}}(n)e(n); \qquad (14)$$

and

$$\mathbf{x}_{\hat{C}}(n) = \left[\sum_{i=0}^{I-1} \hat{c}_i x(n-i), \ldots, \sum_{i=0}^{I-1} \hat{c}_i x(n-i-M+1) \right]^T, \qquad (15)$$

where μ is the adaptation step size and γ is the leakage coefficient $0 < \gamma < 1$, usually selected close to unity. By selecting $\gamma = 1$ the feedback filtered-x LMS algorithm is obtained. Furthermore, $\mathbf{x}_{\hat{C}}(n)$ is the filtered reference signal vector, which usually is produced by filtering the reference signal $x(n)$ with an I-coefficients FIR-filter estimate, $\hat{c}_i$, $i \in 0, 1, \ldots, I-1$, of the control path or plant. Furthermore, $\mathbf{w}(n)$ is the adaptive FIR filter coefficient vector, $y(n)$ is the output signal from the adaptive FIR filter, $e(n)$ is the error signal, $y_C(n)$ the secondary vibration (the output signal from the plant), $\hat{C}$ is an estimate of the forward path and $d(n)$ is the primary disturbance. The reference signal vector $\mathbf{x}(n) = [x(n), x(n-1), \ldots, x(n-M+1)]^T$ is related to the error signal as $x(n) = e(n-1)$.[15,16,31] In order to select a step size μ to enable the feedback filtered-x LMS algorithm to converge, the inequality $0 < \mu < 2/(E[x_{\hat{C}}^2(n)](M+\delta))$ may be used,[15,16,31] where δ is the overall delay in the forward path, M is the length of the adaptive FIR filter and $E[x_{\hat{C}}^2(n)]$ is the mean square value of the filtered reference signal to the algorithm. Incorporating a leakage factor γ in the feedback filtered-x LMS-algorithm causes the loop gain of the control system to be reduced, yielding a more robust behaviour.[15,16]

3. RESULTS

3.1. The Plant

The system to be controlled, C, is comprised of several parts: a signal conditioning filter, an actuator amplifier, an actuator, the structural path between the force applied by actuator on the boring bar, and the boring bar response (measured by an accelerometer mounted close to the tool-tip). In order to clamp the boring bar, it is first inserted into the cylindrical space of the clamping house. It is then clamped by means of four/six clamping screws; two/three on the tool side and two/three on the opposite side of the boring bar. The two standard versions of the clamping house are distinguishable only by the fact that one supports four clamping screws while the other supports six. It is obvious that the boundary conditions applied by the four-screw version of the clamping house will differ from the boundary conditions applied by the six-screw version of the clamping house. Also, to enable the boring bar to be inserted in the clamping house, the diameter of the clamping house's cylindrical clamping space is slightly larger than the diameter of the boring bar. Thus, the exact spatial position of the clamped boring bar end in the clamping space of the clamping house is difficult to pinpoint. Furthermore, the tightening torque of the clamping screws, i.e. the clamping force, is likely to vary between the screws each time the boring bar is clamped and each screw is tightened. Thus, each time the boring bar is clamped it is likely that the clamped boring bar will have different dynamic properties.

Plant frequency function estimates were produced when the boring bar was not in contact with the workpiece, i.e. off-line. The control path was estimated off-line for ten different possible clamping conditions with respect to the tightening torque of the screws and the spatial position of the boring bar in the clamping space of the clamping house. Two spatial positions within clamping space were selected. The first was

that in which the upper side of the boring bar's end (the tool side) was clamped in contact with the upper section of the clamping space surface. The second was that in which the opposite, underside of the boring bar's end, was clamped in contact with the lower section of the clamping space surface. For each of these two spatial position configurations, five various tightening torques were used. The different off-line clamping conditions are presented by Table 2.

Table 2. The ten different clamping conditions of the boring bar used for the production of plant estimates when the boring bar is not in contact with the workpiece (off-line). Four clamping screws were used, two on the tool side and two on the opposite side.

Notation	Torque (Nm)	Contact
BC_1	10	
BC_2	20	
BC_3	30	Boring bar in contact with upper side to clamping housing
BC_4	40	
BC_5	50	
BC_6	10	
BC_7	20	
BC_8	30	Boring bar in contact with under side to clamping housing
BC_9	40	
BC_{10}	50	
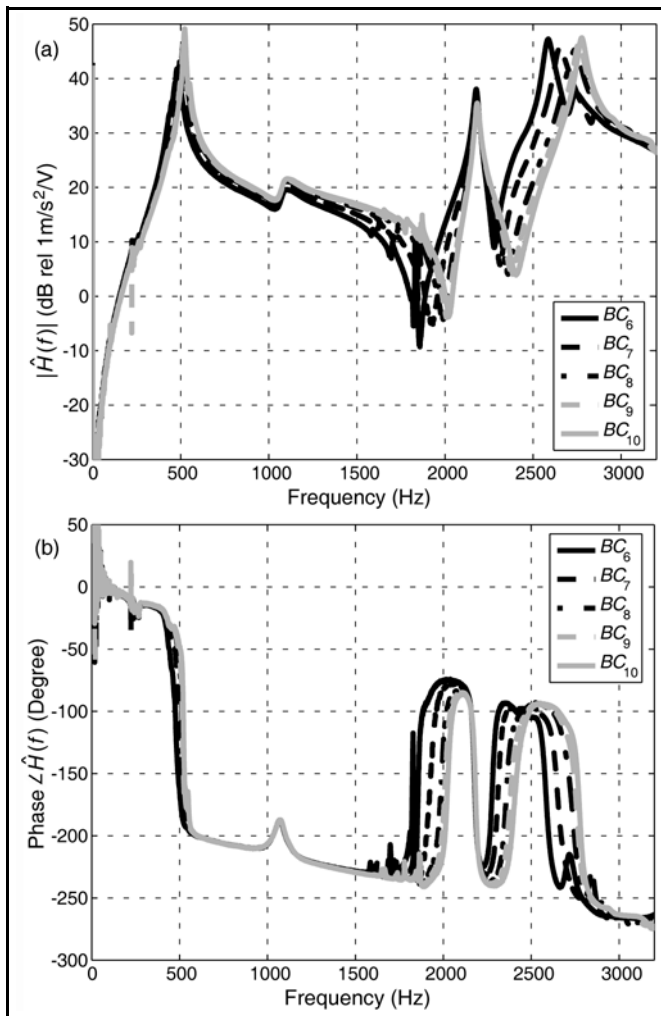
Figure 13. Frequency function estimates of the plant, for the five different tightening torques of the clamping screws, when the underside, of the boring bar end, is clamped in contact with the lower part of the clamping space surface.

The spectrum estimation parameters and identification signal used in the production of off-line frequency function estimates are given in Table 1 column A. Figure 13 shows frequency function estimates of the plant for five different clamping screw tightening torques ($BC_6 - BC_{10}$). These plant frequency function estimates are shown in the frequency range of the fundamental resonance frequency of the boring bar in Fig. 14.
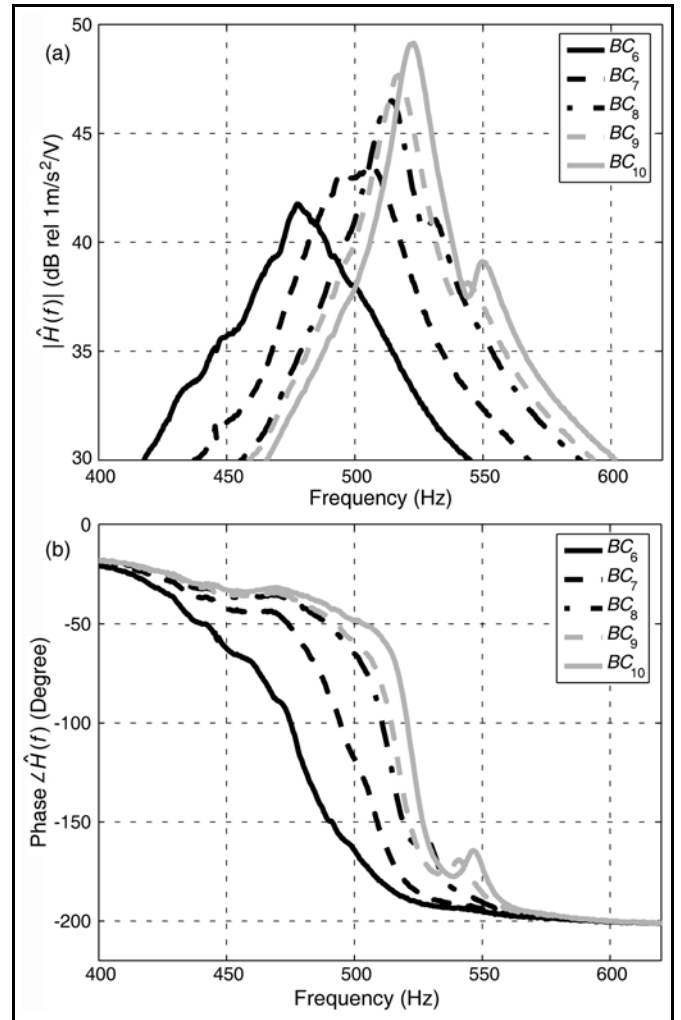
Figure 14. Frequency function estimates of the plant in the frequency range of the fundamental resonance frequency of the boring bar, for the five different tightening torques clamping screws, when the underside, of the boring bar end is clamped in contact with the lower part of the clamping space surface.

The five other plant estimates shows similar differences but with the resonance frequency peak between 450 to 470 Hz. As opposed to a situation in which the boring bar is not in contact with the workpiece, contact with the workpiece during a continuous cutting operation will cause the boundary conditions on the cutting tool to change.[4,5] Hence, the dynamic properties of the plant will be different when the boring bar is not in contact with the workpiece and during continuous turning. Also, different cutting data and work material are likely to affect the dynamic properties of the plant during continuous turning.[4,5] Plant frequency function estimates were produced during continuous turning for a variety of different cutting data. The clamping conditions with respect to the tightening torque of the clamping screws and the spatial position of the boring bar in the clamping space of the

clamping house were fixed and are given by clamping condition BC_{10} in Table 2. The spectrum estimation parameters and identification signal used in the production of on-line frequency function estimates are given in Table 1 column B.

Figure 15 presents two different plant frequency function estimates produced during continuous turning (on-line) with different cutting data (see Table 3). This diagram also present a plant frequency function estimate produced when the boring bar is not in contact with the workpiece (off-line). The off-line frequency function estimate was produced using the spectrum estimation parameters and identification signal according to Table 1 column A.

Table 3. Cutting data used for plant frequency response function estimation during continuous turning (on-line).

Notation	Cutting parameters		
	Cutting depth (mm)	Cutting speed (m/min)	Feed rate (mm/rev)
On-line 1	1.2	80	0.2
On-line 2	1	150	0.2
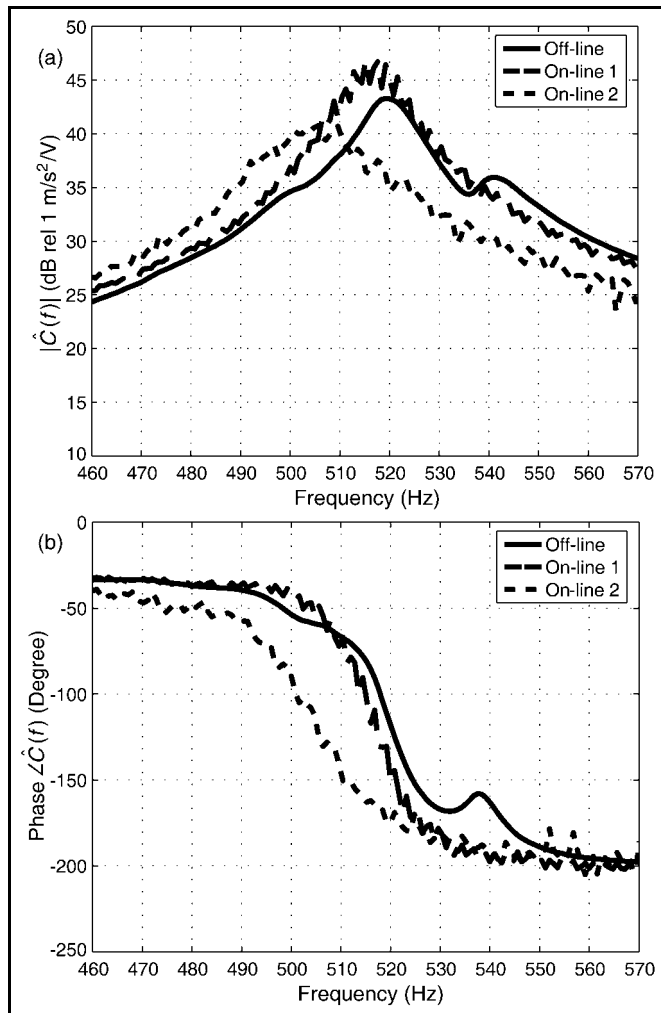
Figure 15. Frequency function estimates of the plant during a continuous cutting operation (online) and when the boring bar is not in contact with the workpiece (off-line). The on-line estimation of the plant was produced using workpiece material SS2541-03, cutting tool DNMG 150806-SL, grade TN7015. On-line 1: feed rate $s = 0.2$ mm/rev, cutting depth $a = 1.2$ mm, cutting speed $v = 80$ m/min and On-line 2: feed rate $s = 0.2$ mm/rev, cutting depth $a = 1$ mm, cutting speed $v = 150$ m/min.

The coherence functions corresponding to both the on-line control path frequency response function estimates and the off-line estimates are shown in Fig. 16 (a). Estimates of the random error for the on-line and off-line frequency response function estimates in Fig. 15 are shown in Fig. 15 (b).
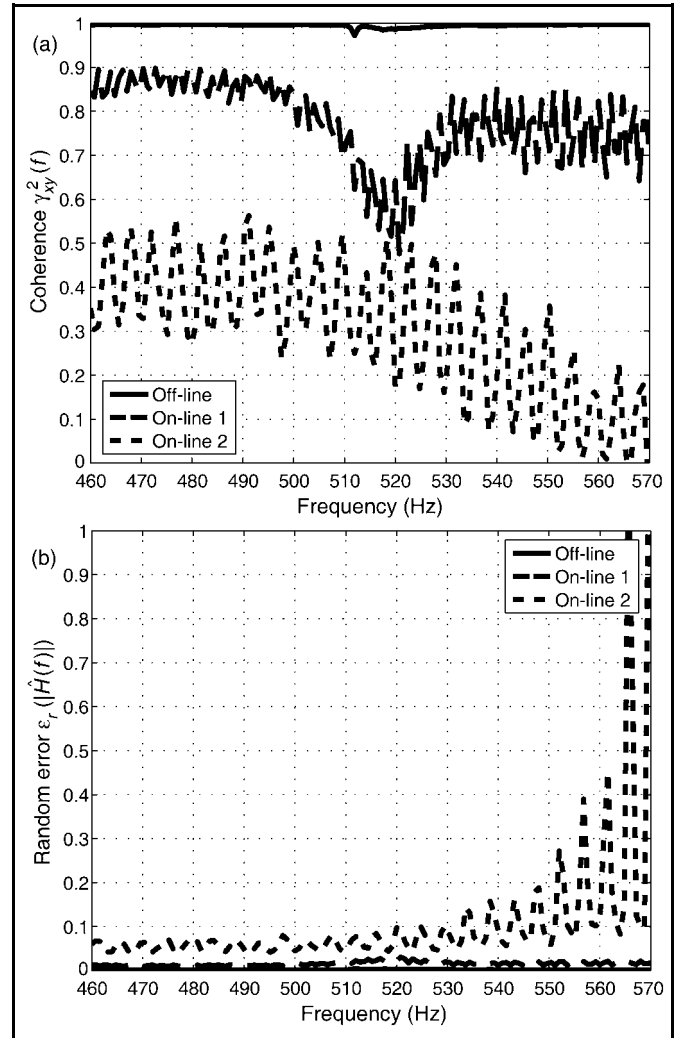

Figure 16. (a) Coherence function estimates between input and output signal of the plant during continuous cutting (on-line) and when the boring bar is not in contact with the workpiece (off-line). (b) Estimate of the random error for the on-line and off-line frequency response function estimates.

3.2. Active Boring Bar Vibration Control Results

The cutting experiments utilised three different feedback controllers in the active control of boring bar vibration: first, an analog manually adjustable controller based on lead compensation; secondly, a manually adjustable analog stand alone controller, based on a lead-lag compensation; and finally an adaptive digital controller based on the feedback filtered-x LMS algorithm. To illustrate the results of the active control of boring bar vibration using the three different controllers, power spectral densities of boring bar vibration with and without active vibration control are presented in the same diagram. The spectrum estimation parameters used in the production of boring bar vibration power spectral density estimates are shown in Table 1 column D.

Initially, a simple analog manually adjustable lead compensator, based on digitally controlled analog design was developed. The adjustable lead compensator was tuned manu-

ally and it was possible to provide an attenuation of the boring bar vibration level by up to approximately 35 dB. However, using the manually adjustable lead compensator in the active control of boring bar vibration frequently resulted in stability problems. By using the manually adjustable band-pass lead-lag controller in the active control of boring bar vibration, the vibration level was reduced by up to approximately 50 dB after a simple manual tuning of the controller (see Fig. 17). Furthermore in numerous cutting experiments, the active control of boring bar vibration based on the band-pass lead-lag controller after initial manual tuning has provided stable control with significant vibration attenuation.
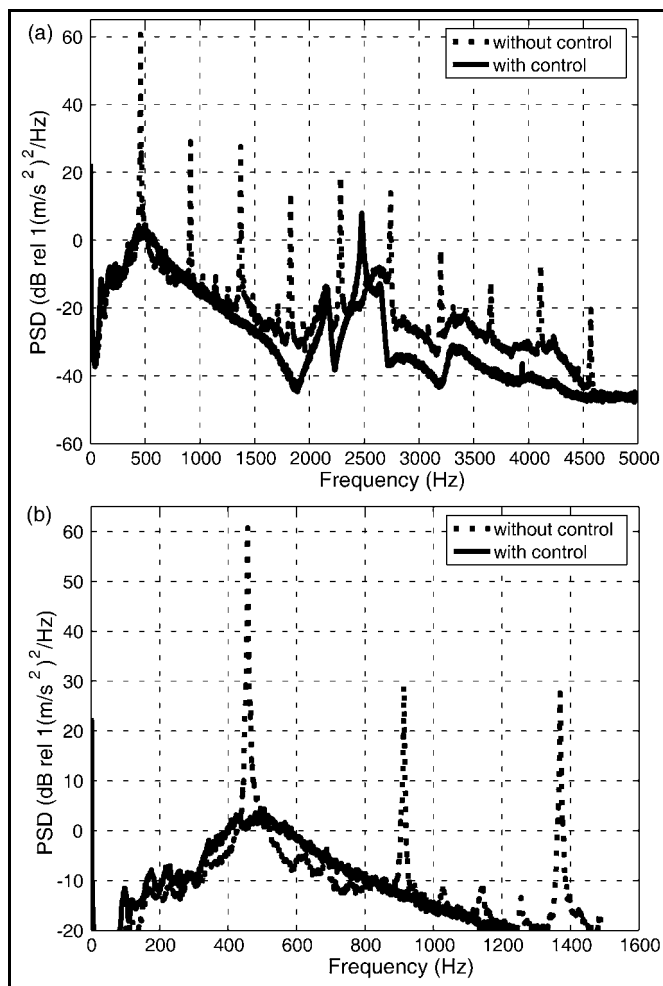
Figure 17. (a) Power spectral densities of boring bar vibration in the cutting speed direction with active control using the adjustable lead-lag controller (solid line) and without active control (dashed line). (b) The corresponding spectra zoomed in to the three first resonance peaks. Workpiece material SS2541-03, cutting tool DNMG 150806-SL, grade TN7015, feed rate $s = 0.24$ mm/rev, cutting depth $a = 2$ mm, cutting speed $v = 60$ m/min.

By utilising the feedback filtered-x LMS algorithm as controller in the active control of boring bar vibration, the adaptive controller will tune the adaptive FIR filter to decorrelate the error signal with the filtered reference signal vector. Therefore, high loop gain is provided in the frequency range of the resonance frequency that dominates the boring bar vibration. Frequently, at high boring bar vibration levels, the feedback filtered-x LMS algorithm in the active control of boring bar vibration yields an attenuation of the vibration by more than 50 dB at the dominating resonance frequency. However, feedback filtered-x LMS algorithm requires leakage to provide stable and robust control[15,31] and the cost for improved robustness is a somewhat reduced vibration attenuation performance.

3.3. Stability and Robustness of the Controllers

The stability of a feedback control system requires that its open loop frequency response $H_{ol}(f)$ does not violate the closed loop stability requirements, i.e. the Nyquist stability criterion.[22,28,29] A closed loop system is said to be stable if the polar plot of the open loop frequency response $H_{ol}(f)$ for the feedback control system does not enclose the $(-1, 0)$ point in the Nyquist diagram. The greater the shortest distance between the polar plot and the $(-1, 0)$ point, the more robust the feedback control system is with respect to variation in plant response and controller response. The system fulfils the conditions for robust stability[22,28,29] if there is no phase function present which (in combination with maximal magnitude of the possible plant uncertainties at each frequency) can result in a feedback control system open loop frequency response that encloses the $(-1, 0)$ point in the Nyquist diagram.

An estimate of the open loop frequency function for a feedback control system may be produced based on the controller frequency response function and the plant frequency response function. The analog controller frequency response function was estimated after manually tuning for active control of boring bar vibration. In the case of the adaptive digital controller, the controller frequency response function was estimated after convergence with the step size set to zero. All the controllers were estimated with the spectrum estimation parameters and the identification signal shown in Table 1 column C. The open loop frequency responses for the active boring bar vibration control system were produced for the manually adjustable lead compensator and the off-line control path frequency function estimate for each of the ten different clamping conditions of the boring bar (see Table 2). Also, the open loop frequency responses for the manually adjustable lead compensator and the two different on-line plant frequency function estimates were produced. Observe that in order to facilitate interpretation of the Nyquist diagrams, the number of the open loop frequency response functions plotted in the same diagram were limited to four. These open loop frequency response functions were selected in order to avoid redundancy in the Nyquist diagrams and to form the open loop frequency response functions. The plant frequency response function estimates corresponding to the clamping conditions (BC_1, BC_5, BC_6 and BC_{10}) were selected (see Table 2). The Nyquist diagram in Fig. 18 shows polar plots of the selected open loop frequency responses. The corresponding Bode plot is shown in Fig. 19.

Observe, in Fig. 18, that the polar plots of the open loop frequency responses for the feedback control system based on the manually adjustable lead compensator are close to, or enclose, the $(-1, 0)$ point in the Nyquist diagram. Figure 19 demonstrates that open loop frequency responses for the boring bar vibration control system based on the manually adjustable lead compensator provide substantial loop gain at resonance frequencies above 2000 Hz. Open loop frequency responses for the boring bar vibration control system were produced based on the manually adjustable band-pass lead-lag compensator and the off-line plant frequency function estimate for each of the ten different boring bar clamping conditions (see Table 2).
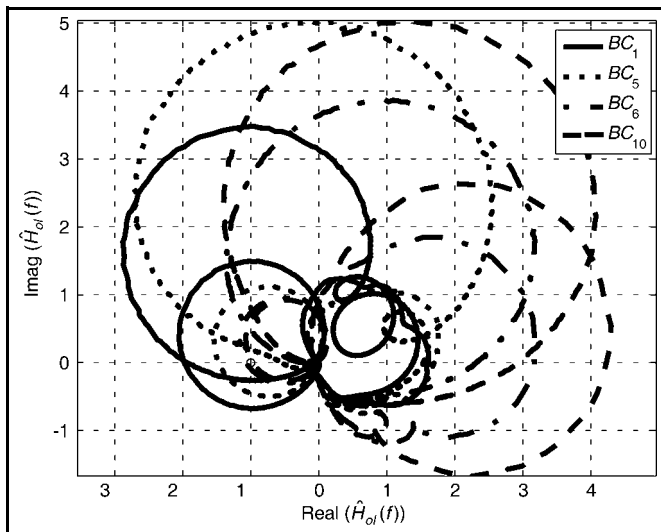
Figure 18. Nyquist diagram for a boring bar vibration control system based on a manually adjustable lead compensator for the four different plant frequency response function estimates corresponding to the clamping conditions: BC_1, BC_5, BC_6 and BC_{10}.
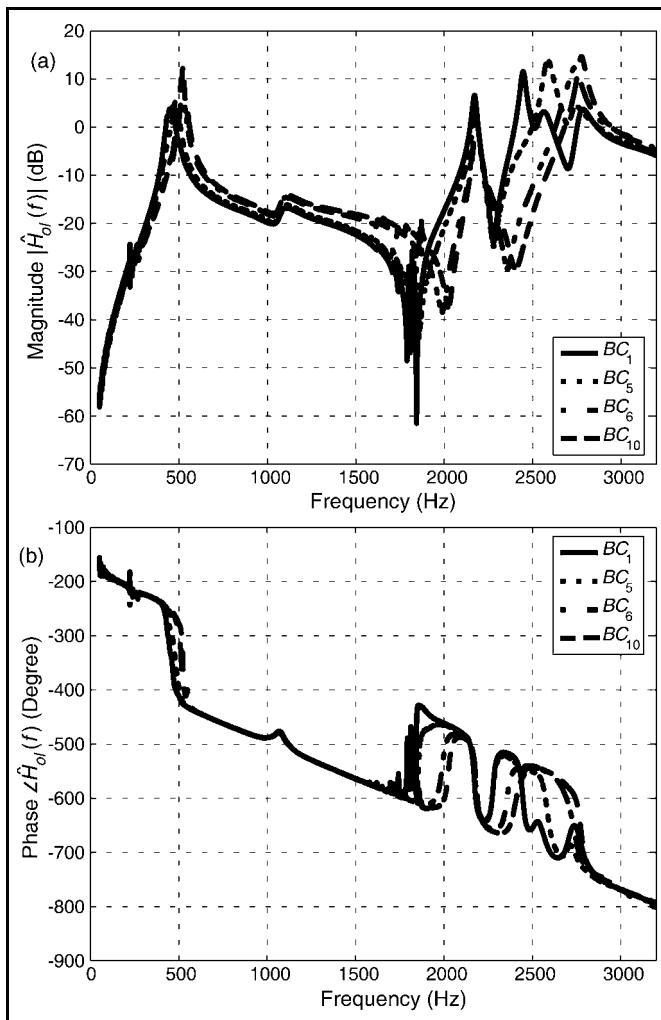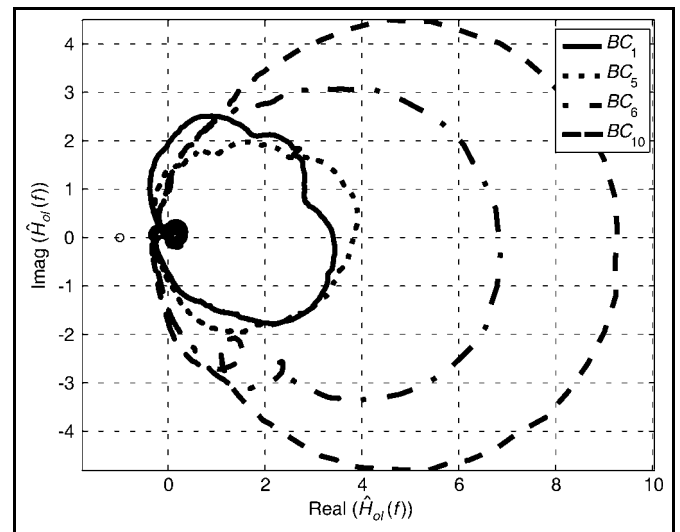

Figure 19. Open loop frequency response function estimates for a boring bar vibration control system, based on a manually adjustable lead compensator for the four different plant frequency response function estimates corresponding to the clamping conditions: BC_1, BC_5, BC_6 and BC_{10}.

Also, open loop frequency responses were produced for the manually adjustable lead compensator and the two differ-

ent on-line control path frequency function estimates. The selected open loop frequency functions for the active boring bar control system based on band-pass lead-lag compensator are shown in the Nyquist diagram in Fig. 20 (these estimates were based on the clamping conditions: BC_1, BC_5, BC_6 and BC_{10}). The corresponding Bode plot of the open loop frequency response functions for the active boring bar control system are shown in Fig. 21.

Observe the distance between the polar plots of the open loop frequency response function estimates for the boring bar vibration control system based on the manually adjustable band-pass lead-lag compensator and the $(-1, 0)$ point in the Nyquist diagram in Fig. 20. In addition, the Bode plot (see Fig. 19) demonstrates low loop gain above 1000 Hz.
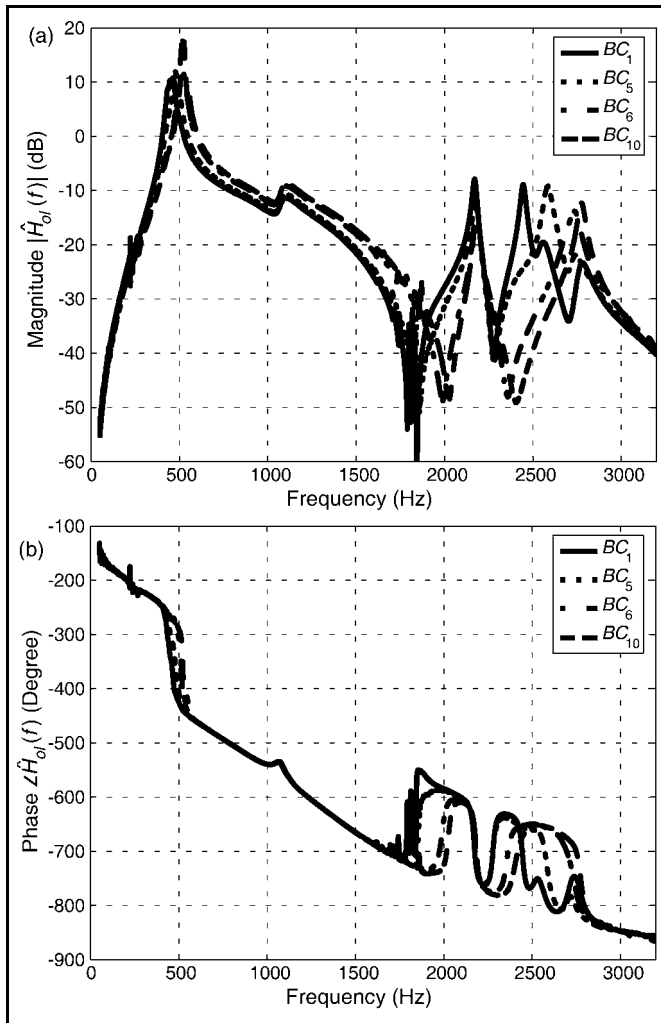

Figure 20. Nyquist diagram for a boring bar vibration control system, based on a manually adjustable band-pass lead-lag compensator for the four different plant frequency response function estimates corresponding to the clamping conditions: BC_1, BC_5, BC_6 and BC_{10}.

The adaptive digital control of boring bar vibration was carried out with and without a leakage factor in the feedback filtered-x LMS algorithm. The Nyquist diagram in Fig. 22 shows the polar plots of the four open loop frequency responses, which is based on the feedback filtered-x LMS algorithm. The four open loop frequency functions for the active boring bar control system based on the feedback filtered-x LMS algorithm are shown in the Nyquist diagram in Fig. 22.
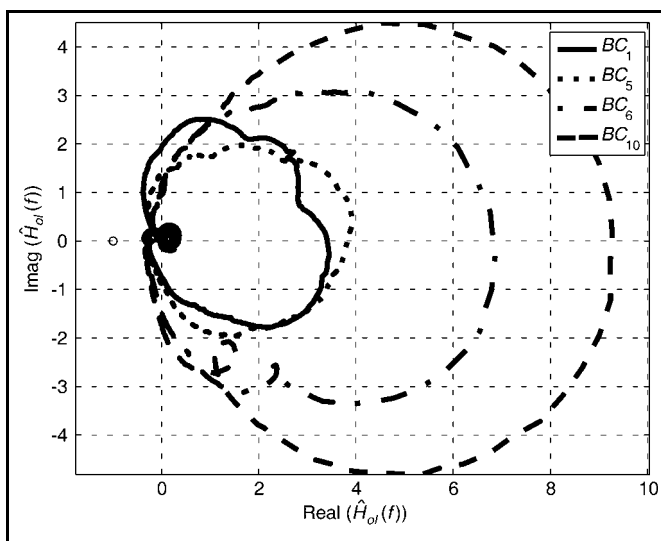
The corresponding Bode plots of the open loop frequency response functions based on the feedback filtered-x LMS algorithm are shown in Fig. 23.

The feedback filtered-x LMS algorithm will automatically tune the adaptive FIR filter to de-correlate the error signal with the filtered reference signal vector. Thus, a high loop gain will be provided in the frequency range of the resonance frequency that dominates the boring bar vibration (see the Bode plot in Fig. 23). Finally, the leaky feedback filtered-x LMS controller yields a significantly lower loop gain compared to the case of no leakage.

If, for example, the plant frequency function estimate corresponding to the clamping condition BC_{10} is selected as a nominal control path or plant model of the plant then an estimate of the upper bound $\beta(f)$ for the multiplicative perturbation modelling the plant uncertainty may be produced based on Eq. (6) using all the other plant frequency function estimates (not the plant frequency function estimate correspond-

Figure 21. Open loop frequency response function estimates, for a boring bar vibration control system, based on a manually adjustable band-pass lead-lag compensator for the four different plant frequency response function estimates corresponding to the clamping conditions: BC_1, BC_5, BC_6 and BC_{10}.

Figure 22. Nyquist diagram for a boring bar vibration control system, based on the feedback filtered-x LMS algorithm for the four different plant frequency response function estimates, corresponding to the clamping conditions: BC_1, BC_5, BC_6 and BC_{10}. Number of adaptive filter coefficients $M = 20$, step size $\mu = -0.5$, sampling frequency of the DSP $F_s = 8$ kHz.
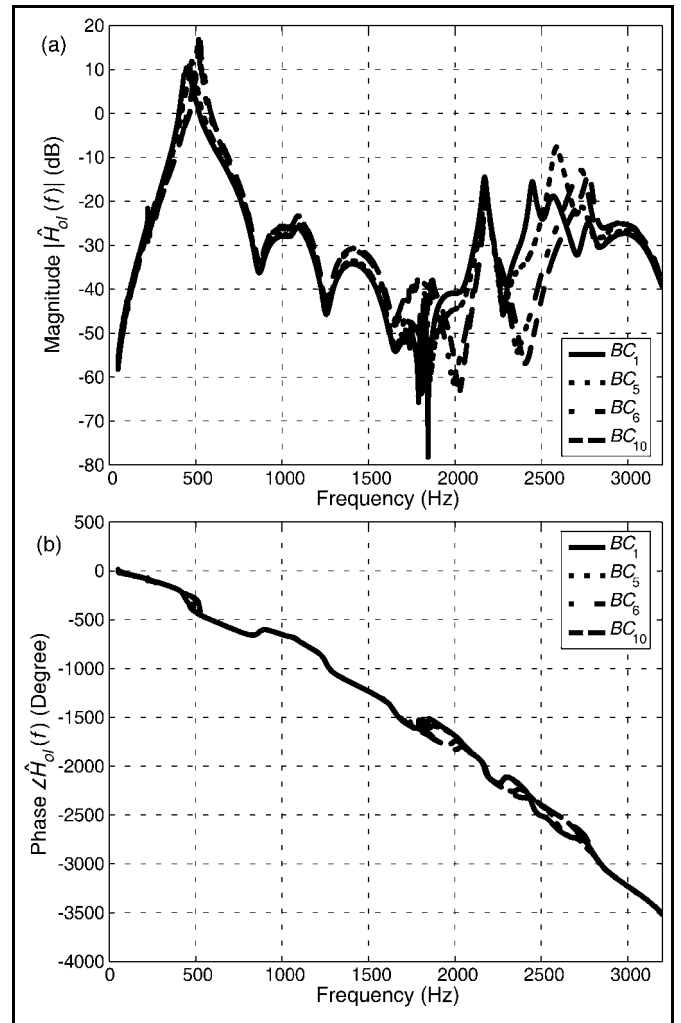
Figure 23. Open loop frequency response function estimates for a boring bar vibration control system, based on the feedback filtered-x LMS algorithm for the four different plant frequency response function estimates, corresponding to the clamping conditions: BC_1, BC_5, BC_6 and BC_{10}. Number of adaptive filter coefficients $M = 20$, step size $\mu = -0.5$, sampling frequency of the DSP $F_s = 8$ kHz.
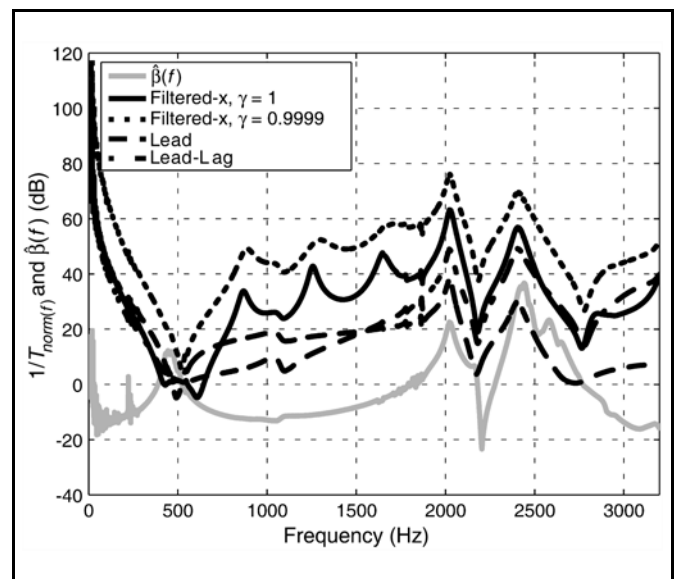
Figure 24. Magnitude of the inverse of the nominal complementary function for each of the controllers and the estimated upper bound for the multiplicative perturbation.

ing to the clamping condition BC_{10}). In Fig. 24 the magnitude of the inverse of the nominal complementary function for each of the controllers is plotted in the same diagram as the estimated upper bound $\hat{\beta}(f)$ for the multiplicative perturbation.

4. DISCUSSION AND CONCLUSIONS

The above results demonstrate that boring bar vibration in internal turning may be reduced by utilising active control based on active boring bars with embedded actuator and sensor and a suitable feedback controller such as an analog manually adjustable band-pass lead-lag controller or an adaptive digital controller based on the feedback filtered-x LMS algorithm. It has been established that for each time the boring bar is clamped, it is likely that the clamped boring bar will have different dynamic properties (see Figs. 13 and 14). Also, the dynamic properties of the clamped boring bar will differ between these instances when the boring bar is not in contact with the workpiece and during continuous turning (see Fig. 15). In addition, different cutting data and work materials will likely affect the dynamic properties of the clamped boring bar during continuous turning.[4] Thus, the plant in the active boring bar vibration system may display significant variations in its dynamic properties. Hence, a robust controller that performs well for substantial variations in the dynamics of the plant is required for the active control of boring bar vibration.

The development of a simple adjustable analog controller, based on digitally controlled analog design, started initially with a lead compensator. However, the vibration to be controlled is related to the fundamental bending modes of the boring bar and not its higher order modes.[4,5] Thus, the high loop gain (provided by a controller above the fundamental bending modes eigenfrequencies) will likely be an issue concerning the stability and robustness of the active boring bar vibration control system. However if the manually adjustable lead control is utilised for active boring bar vibration control, it will (when stable) perform a broad-band attenuation of the tool-vibration. Therefore, the vibration level is reduce by over 35 dB at 460 Hz and harmonics of the 460 Hz boring bar resonance frequency are attenuated. The reduction of the harmonics of the dominating fundamental resonance frequency is probably a consequence of a linearisation of the boring bars dynamic response imposed by the active vibration control. Polar plots of the open loop frequency responses (for the feedback control system based on the manually adjustable lead compensator), which approach or enclose the $(-1, 0)$ point of the Nyquist diagram, also demonstrate problems with robustness and stability (see Fig. 18). According to the Bode plots (Fig. 19), the manually adjustable lead compensators provides (as expected) a substantial loop gain at the boring bar resonance frequencies above 2000 Hz. Thus, to provide high boring bar vibration attenuation, high loop gain is only required in the frequency range of the boring bar's fundamental bending modes eigenfrequencies. Basically, a manually adjustable controller should be able to provide adjustable band-pass gain and adjustable phase enabling to control the plant in the frequency range of the boring bar's fundamental bending modes eigenfrequencies. This will produce adequate anti-vibration cancelling the original vibration excited by the material deformation process.

The adaptive digital feedback control based on feedback filtered-x LMS algorithm (with and without leakage) performs a broad-band attenuation of tool-vibration and is able to reduce vibration levels by over 50 dB at 460 Hz, as well as to attenuate the harmonics of the 460 Hz boring bar resonance frequency. However, slightly lower vibration attenuation might be observed for the leaky feedback filtered-x LMS algorithm. The introduction of a leakage factor or a "forgetting factor" in the feedback filtered-x LMS algorithm's recursive coefficient adjustment algorithm will provide a restraining influence on the loop gain of the control system and may thereby cause a somewhat reduced attenuation of the boring bar vibration.

The active boring bar vibration control system based on the manually adjustable band-pass lead-lag control performs a broad-band attenuation of tool-vibration and is also able to reduce the vibration level by over 50 dB at 460 Hz, as well as to attenuate the harmonics of the 460 Hz boring bar resonance frequency (see Fig. 17). Thus, the band-pass lead-lag controller provides attenuation performance comparable to that of the adaptive controller by tuning the adaptive FIR filter to de-correlate the error signal with the filtered reference signal vector. It thereby provides high loop gain in the frequency range of the resonance frequency that dominates the boring bar vibration (see Fig. 23). By comparing the loop gains provided by the adaptive digital controller with the loop gains provided by the band-pass lead-lag controller (see Fig. 19), it follows that the analog lead-lag controller is tuned to provide high loop gain over a broader frequency range as compared to the loop gain resulting from the adaptive digital control. On the other hand, by examining the Nyquist plots for the open loop frequency response functions concerning the band-pass lead-lag controller (see Fig. 20) and the feedback filtered-x LMS controller (see Fig. 22), it follows that the shortest distance between the polar plots and the $(-1, 0)$ point is greater for the analog controller as compared with the feedback filtered-x LMS controller.

If robust stability is considered (see Fig. 24), it follows that the active boring bar vibration control system based on the leaky feedback filtered-x LMS controller is the only system that fulfils the conditions for robust stability. It is also the controller that results in the greatest shortest distance between the polar plots and the $(-1, 0)$ point. However, the active boring bar vibration control system based on the band-pass lead-lag controller, tuned initially, remained stable during the course of numerous trials with varied clamping conditions and cutting data.

Acknowledgements

REFERENCES

[1] Revin E. I. Tooling structure: Interface between cutting edge and machine tool, *Annals of the CIRP*, **49** (2), 591-634, (2000).

[2] Håkansson, L., Johansson, S., and Claesson, I. Chapter 78 - Machine tool noise, vibration and chatter prediction and control, *Handbook of Noise and Vibration Control*, Malcolm J. Crocker (ed.), submited for publication in John Wiley & Sons, (2005).

[3] Sandvik. *Modern metal cutting - a practical handbook*, AB Sandvik Coromant, 1st edition, (1994).

4 Andrén, L., Håkansson, L. Brandt, A., and Claesson, I. Identification of dynamic properties of boring bar vibrations in a continuous boring operation, *Journal of Mechanical Systems & Signal Processing*, **18** (4), 869-901, (2004).

5 Andrén, L., Håkansson, L. Brandt, A., and Claesson, I. Identification of motion of cutting tool vibration in a continuous boring operation - correlation to structural properties, *Journal of Mechanical Systems & Signal Processing*, **18** (4), 903-927, (2004).

6 Pettersson, L., Håkansson, L., Claesson, I., and Olsson, S. Active control of boring bar vibration in cutting operations, *Proceedings of the Ninth International Congress on Sound and Vibration*, (2002).

7 Åkesson, H., Smirnova, T., Håkansson, L., Claesson, I., and Lagö, T. Analog versus digital control of boring bar vibration, SAE World Aerospace Congress (WAC), Dallas, Texas, 3-6 October, (2005).

8 Ruud, N. A., Karlsen, R., Sorby, K., and Richt, C. Minimizing vibration tendencies in machining, Technical Article at http://www.coromant.sandvik.com, (2005).

9 Claesson, I., and Håkansson, L. Active control of machine-tool vibration in a lathe, *Proceedings of the Fifth International Congress on Sound and Vibration*, (1997).

10 Tewani, S. G., Rouch, K. E., and Walcott, B. L. Active control of machine tool chatter for a boring bar: experimental results, *Proceedings of ASME, Vibration and Control of Mechanical Systems*, **DE-Vol. 61**, 103-115, (1993).

11 Tewani, S. G., Rouch, K. E., and Walcott, B. L. A study of cutting process stability of a boring bar with active dynamic absorber, *International Journal of Machine Tools & Manufacture*, **35** (1), 91-108, (1995).

12 Browning, D. R., Golioto, I., and Thompson, N. B. Active chatter control system for longoverhang boring bars, *Proceedings of SPIE*, **3044**, 270-280, (1997).

13 Pettersson, L., Håkansson, L., Claesson, I., and Olsson, S. Control of machine-tool vibration in a cnc lathe based on an active tool holder shank with embedded piezo ceramic actuators, *Proceedings of the Eight International Congress on Sound and Vibration*, (2001).

14 Åkesson, H., Smirnova, T., Håkansson, L., Claesson, I., Sigfridsson, A., Svensson, T., and Lagö, T. A first prototype of an active boring bar tested in industry, *Proceedings of the Thirteenth International Congress on Sound and Vibration*, (2006).

15 Claesson, I. and Håkansson, L. Adaptive active control of machine-tool vibration in a lathe, *International Journal of Acoustics and Vibration*, **3** (4), 155-162, (1998).

16 Håkansson, L., Johansson, S., Dahl, M., Sjösten, P., and Claesson, I. Chapter 12 - Noise canceling headsets for speech communication, *CRC Press Handbook on Noise Reduction in Speech Applications*, Gillian M. Davis (ed.). CRC Press, (2002).

17 Fuller, C. R., Elliott, S. J., and Nelson, P. A. *Active control of vibration*, Academic Press, Inc, (1996).

18 Doyle, J. F. *Wave propagation in structures - spectral analysis using fast discret fourier transforms*, Springer, second edition, (1997).

19 Hansen, C. H. and Snyder, S. C. *Active control of noise and vibration*, E & FN SPON, (1997).

20 Inman, D. J. *Engineering vibration*, Prentice-Hall, second edition, (2001).

21 Han, S. M., Benaroya, H., and Wei, T. Dynamics of transversely vibrating beams using four engineering theories, *Journal of Sound and Vibration*, **225** (5), 935-988, (1999).

22 Franklin, G. F., Powell, J. D., and Emami-Naeini, A. *Feedback control of dynamic systems*, Addison Wesley, third edition, (1994).

23 Doyle, J. C., Francis, B. C., and Tannenbaum, A. R. *Feedback control theory*, Macmillan, (1992).

24 Bendat, J. S. and Piersol, A. G. *Random data analysis and measurement procedures*, John Wiley & Sons, third edition, (2000).

25 Welch, P. D. The use of fast fourier transform for the estimation of power spectra: a method based on time averaging over short, modified periodograms, *IEEE Transactions on Audio and Electroacoustics*, 70-73, June, (1967).

26 Franklin, G. F., Powell, J. D., and Emami-Naeini, A. *Feedback control of dynamic systems*, Prentice Hall, fifth edition, (2006).

27 Elliott, S. J. and Sutton, T. J. Performance of feedforward and feedback systems for active control, *IEEE Transactions on Speech and Audio Processing*, **4** (3), 214-223, (1996).

28 Elliott, S. J. *Signal processing for active control*, Academic Press, London, first edition, (2001).

29 Dorf, R. C. and Bishop, R. H. *Modern control systems*, Prentice Hall, tenth edition, (2005).

30 Beale, G. Phase lead compensator design using bode plots, Course Literature at: http://ece.gmu.edu/ gbeale/ece_421, (2005).

31 Andrén, L., Håkansson, L. and Claesson, I. Active control of machine tool vibration in external turning operations, *Proceedings of the Institution of Mechanical Engineers, Part B, Journal of Engineering Manufacture*, **217** (B6), 869-872, (2003).